Editors' Suggestion

Planar Hall Effect in Quasi-Two-Dimensional Materials

Koushik Ghorai,* Sunit Das,* Harsh Varshney, and Amit Agarwal†
Department of Physics, Indian Institute of Technology Kanpur, Kanpur-208016, India

(Received 12 May 2024; accepted 26 November 2024; published 13 January 2025)

The planar Hall effect in 3D systems is an effective probe for their Berry curvature, topology, and electronic properties. However, the Berry curvature-induced conventional planar Hall effect is forbidden in 2D systems as the out-of-plane Berry curvature cannot couple to the band velocity of the electrons moving in the 2D plane. Here, we demonstrate a unique 2D planar Hall effect (2DPHE) originating from the hidden planar components of the Berry curvature and orbital magnetic moment in quasi-2D materials. We identify all planar band geometric contributions to 2DPHE and classify their crystalline symmetry restrictions. Using gated bilayer graphene as an example, we show that in addition to capturing the hidden band geometric effects, 2DPHE is also sensitive to the Lifshitz transitions. Our Letter motivates further exploration of hidden planar band geometry-induced 2DPHE and related transport phenomena for innovative applications.

DOI: 10.1103/PhysRevLett.134.026301

Introduction—The planar Hall effect (PHE) is the generation of longitudinal and transverse voltages in the plane of the applied electric (***E***) and magnetic fields (***B***). In contrast to the conventional and anomalous Hall effect, the transport in PHE is dissipative, and the response typically varies quadratically with the B. PHE has extensive applications in magnetic sensors and memory devices [1]. In 3D materials, PHE generally originates from the coupling of the Berry curvature (BC) and orbital magnetic moment (OMM) to the band velocity and in-plane magnetic field, respectively. Initial studies of PHE used it effectively to probe the magnetization reversal in magnetic materials [2–6]. More recently, PHE has been used to explore novel topological semimetals [7–18] and topological insulators [19,20].

However, conventional PHE probes are ineffective in 2D systems. As the 2D plane confines the orbital motion of electrons, these systems can host only out-of-plane Berry curvature and orbital magnetic moment [21–24]. Consequently, the PHE induced by the component of the BC and OMM in the plane of the applied electric and magnetic field is forbidden in perfect 2D systems. Some 2D materials with strong spin-orbit coupling exhibit an intrinsic magneto-Hall response driven by magnetic field-induced changes to the Berry curvature [25–31] and asymmetric spin scaterring [32–39]. However, such responses are absent in systems lacking strong spin-orbit interactions. These limitations severely restrict our ability to utilize PHE to explore fundamental physics and develop ultra-sensitive magnetic sensors and other applications in 2D materials.

*These authors contributed equally to this work.
†Contact author: amitag@iitk.ac.in

In this Letter, we introduce a unique 2D planar Hall effect (2DPHE) in layered 2D materials such as bilayer graphene. Layered 2D materials with finite interlayer tunneling can host an intrinsic in-plane component of the BC and OMM if the system's space inversion or time-reversal symmetry is broken [40–42]. We demonstrate that these relatively unexplored in-plane components of the band geometric quantities induce the 2DPHE response (see Fig. 1). We present a thorough analysis of the 2DPHE responses, particularly their angular variation (angle between ***E*** and ***B***), and classify the crystalline symmetry restrictions on the different 2DPHE response tensors. As an illustrative example, we focus on Bernal stacked bilayer graphene to demonstrate a sizable and gate-tunable 2DPHE response. Beyond predicting the unique phenomena of 2DPHE, our findings motivate the exploration of other

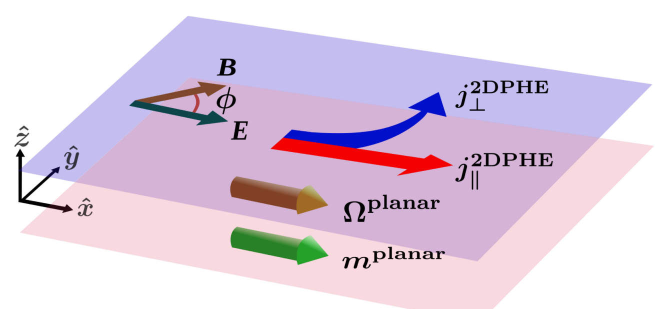

FIG. 1. Schematic for 2D planar Hall effect (2DPHE). Layered 2D materials host hidden planar Berry curvature ($\boldsymbol{\Omega}^{\mathrm{planar}}$) and planar orbital magnetic moment ($\boldsymbol{m}^{\mathrm{planar}}$) arising from interlayer tunneling. The $\boldsymbol{\Omega}^{\mathrm{planar}}$ and $\boldsymbol{m}^{\mathrm{planar}}$ combine with the in-plane electric and magnetic field to induce a longitudinal and transverse current in the 2D plane.

transport and optical phenomena induced by the hidden planar band geometric quantities in layered 2D materials [43,44].

Planar BC and OMM in quasi-2D systems—In quasi-2D materials with two or more atomic layers, the finite interlayer hopping amplitude enables the interlayer tunneling of electrons. The interlayer tunneling of electrons gives rise to hidden planar components of the BC and OMM [42]. These are given by

$$\boldsymbol{\Omega}_{n\boldsymbol{k}}^{\text{planar}} = 2\hbar \,\text{Re} \sum_{n' \neq n} \frac{\boldsymbol{v}_{nn'} \times \boldsymbol{\mathcal{Z}}_{n'n}}{(\varepsilon_{n\boldsymbol{k}} - \varepsilon_{n'\boldsymbol{k}})}, \quad (1)$$

$$\boldsymbol{m}_{n\boldsymbol{k}}^{\text{planar}} = e \,\text{Re} \sum_{n' \neq n} \boldsymbol{v}_{nn'} \times \boldsymbol{\mathcal{Z}}_{n'n}. \quad (2)$$

Here, we have defined the velocity matrix elements as $\hbar \boldsymbol{v}_{nn'} = \langle u_{n\boldsymbol{k}} | \nabla_{\boldsymbol{k}} \mathcal{H}_{\boldsymbol{k}} | u_{n'\boldsymbol{k}} \rangle$, with $\boldsymbol{k} = (k_x, k_y)$. $\varepsilon_{n\boldsymbol{k}}$ and $|u_{n\boldsymbol{k}}\rangle$ are the band energy and periodic part of the Bloch wave function for the nth band, respectively. The matrix element of the out-of-plane position operator $\hat{\mathcal{Z}}$ in the eigenbasis of the system's Hamiltonian is $\boldsymbol{\mathcal{Z}}_{nn'} = \hat{z} \langle u_{n\boldsymbol{k}} | \hat{\mathcal{Z}} | u_{n'\boldsymbol{k}} \rangle$. For a generic heterostructure with multiple layers and orbitals, the position operator can be defined as $\hat{\mathcal{Z}} = \sum_l \sum_n z_l |\psi_l^n\rangle \langle \psi_l^n|$, where z_l refers to the z coordinate of the nth atomic orbital basis $|\psi_l^n\rangle$, localized on the lth layer [41,45,46]. Further details on the calculations of planar OMM and planar BC, and the $\hat{\mathcal{Z}}$ operator, are presented in Secs. S1 and S2 of the Supplemental Material, respectively [47]. We emphasize that the planar BC and planar OMM rely on interlayer hybridization of electronic states, which makes the off-diagonal components of $\boldsymbol{\mathcal{Z}}_{nn'}$ finite. We illustrate the emergence of the planar BC and OMM and their symmetry properties in an intuitive way using a 2×2 low energy model [6,51] Hamiltonian of bilayer graphene in Sec. S3 of the Supplemental Material [47].

2D planar Hall effect—In 2D systems, generally, the in-plane magnetic field interacts with electrons primarily through Zeeman coupling to its spin [25–29,31]. In contrast, the planar OMM allows the magnetic field to couple directly to the orbital motion of electrons. This modifies the band energy ($\tilde{\varepsilon}_{n\boldsymbol{k}} = \varepsilon_{n\boldsymbol{k}} - \boldsymbol{m}_{n\boldsymbol{k}}^{\text{planar}} \cdot \boldsymbol{B}$) and the band velocity. More importantly, the planar BC combines with the band velocity to generate a finite chiral magnetic velocity [52] in 2D systems, which is $\propto (\boldsymbol{v}_{n\boldsymbol{k}} \cdot \boldsymbol{\Omega}_{n\boldsymbol{k}}^{\text{planar}}) \boldsymbol{B}$. We show below that these magnetic field-dependent velocities generate a previously unexplored planar Hall effect in 2D systems. See Fig. S3 of the Supplemental Material [47] for more details.

In the semiclassical Boltzmann transport framework, the charge current is given by $\boldsymbol{j} = -e \sum_n \int [d\boldsymbol{k}] \dot{\boldsymbol{r}}_{n\boldsymbol{k}} g_{n\boldsymbol{k}}$. Here, $g_{n\boldsymbol{k}}$ is the nonequilibrium distribution function, $\dot{\boldsymbol{r}}_{n\boldsymbol{k}}$ is the wave-packet velocity, and $[d\boldsymbol{k}] \equiv d^2\boldsymbol{k}/(2\pi)^2$ for 2D systems. Using the expressions of the planar BC and OMM modified $\dot{\boldsymbol{r}}_{n\boldsymbol{k}}$ and $g_{n\boldsymbol{k}}$ up to linear order in the applied electric field, we calculate the planar current density to the first and second orders in the magnetic field strength B (see Sec. S4 of the Supplemental Material [47] for a detailed derivation). We obtain the longitudinal and transverse components of the 2DPHE currents to be

$$j_a = \tau \chi_{ab;c} E_b B_c + \tau \chi_{ab;cd} E_b B_c B_d. \quad (3)$$

Here, τ is the electron scattering time, $\{a, b, c, d\} \in \{x, y\}$ are the 2D Cartesian coordinates, and the Einstein summation convention is implied. The 2DPHE response tensors can be expressed as a sum of the planar BC, planar OMM, and mixed terms,

$$\chi_{ab;c(d)} = \chi_{ab;c(d)}^{\text{BC}} + \chi_{ab;c(d)}^{\text{OMM}} + \chi_{ab;c(d)}^{\text{BC+OMM}}. \quad (4)$$

We obtain the planar BC contributions to be

$$\chi_{ab;c}^{\text{BC}} = -e^2 \int_{n,\boldsymbol{k}} [(v_a \delta_{bc} + v_b \delta_{ac}) \Omega_V - \frac{e}{\hbar} v_a v_b \Omega_c] f_0', \quad (5)$$

$$\chi_{ab;cd}^{\text{BC}} = -\frac{e^2}{2} \int_{n,\boldsymbol{k}} \left[\delta_{ad} \delta_{bc} \Omega_V^2 - \frac{e}{\hbar} (v_a \delta_{bc} + v_b \delta_{ac}) \Omega_d \Omega_V + \frac{e^2}{\hbar^2} v_a v_b \Omega_c \Omega_d \right] f_0' + (c \leftrightarrow d). \quad (6)$$

Here, $\Omega_V \equiv (e/\hbar) \boldsymbol{v}_{\boldsymbol{k}} \cdot \boldsymbol{\Omega}_{\boldsymbol{k}}$ with $\hbar \boldsymbol{v}_{\boldsymbol{k}} = \nabla_{\boldsymbol{k}} \varepsilon_{\boldsymbol{k}}$ being the band velocity without any magnetic field, and δ_{ab} is the Kronecker delta function. For brevity, we have defined $\int_{n,\boldsymbol{k}} \equiv \sum_n \int [d\boldsymbol{k}]$, and we do not explicitly mention the band index n in the physical quantities. We present the expressions for other contributions in Eq. (4) in Sec. S4 of the Supplemental Material [47].

The planar response tensors in Eqs. (5) and (6) are proportional to either $\boldsymbol{v}_{\boldsymbol{k}} \cdot \boldsymbol{\Omega}_{\boldsymbol{k}}$ or, $\hat{\boldsymbol{B}} \cdot \boldsymbol{\Omega}_{\boldsymbol{k}}$ or, the combination of these terms. For a quasi-2D system, all of these terms vanish if we consider only the conventional out-of-plane BC. As a consequence, earlier works missed this phenomenon. This highlights the crucial role of the hidden planar BC and planar OMM in generating the PHE response in quasi-2D systems. Furthermore, the response tensors $\chi_{ab;c}$ and $\chi_{ab;cd}$ are symmetric with respect to its first two indices. Therefore, we have $\sum_a j_a E_a \neq 0$, indicating the dissipative nature of the planar Hall current. Having established the possibility of 2DPHE, we now analyze the restrictions imposed by crystalline point group symmetries on different 2DPHE response tensors.

Crystal symmetry restrictions—The inversion symmetry ($\mathcal{P}$) imposes no constraints as both $\chi_{ab;c}$ and $\chi_{ab;cd}$ represent linear in E responses. However, we find that $\chi_{ab;c}$ is a third rank $\mathcal{T}$-odd axial tensor [53,54], which is forbidden in nonmagnetic systems (see Sec. S5 of Supplemental Material [47] for details). In contrast, $\chi_{ab;cd}$ is a fourth rank $\mathcal{T}$-even polar tensor and is the leading order contribution in nonmagnetic systems. Denoting a general point group operation via $\mathcal{O}$, the $\chi_{ab;c}$ and $\chi_{ab;cd}$ tensors obey the following transformation rules [53]:

$$\chi_{a'b';c'} = \eta_{\mathcal{T}} \det\{\mathcal{O}\}\mathcal{O}_{a'a}\mathcal{O}_{b'b}\mathcal{O}_{c'c}\chi_{ab;c}, \tag{7}$$

$$\chi_{a'b';c'd'} = \mathcal{O}_{a'a}\mathcal{O}_{b'b}\mathcal{O}_{c'c}\mathcal{O}_{d'd}\chi_{ab;cd}. \tag{8}$$

Here, $\eta_{\mathcal{T}} = \pm 1$ is associated with the magnetic point group symmetry transformation: $\eta_{\mathcal{T}} = -1$ ($\eta_{\mathcal{T}} = 1$) for magnetic (nonmagnetic) point group operation $\mathcal{O} \equiv \mathcal{R}\mathcal{T}$ ($\mathcal{O} \equiv \mathcal{R}$), with $\mathcal{R}$ being a spatial operation.

To be specific about the symmetry constraints of the 2DPHE response, we apply the $\boldsymbol{E}$ along the $\hat{\boldsymbol{x}}$ direction, and an in-plane magnetic field at an angle ϕ with $\boldsymbol{E}$, i.e., $(B_x, B_y) = B(\cos\phi, \sin\phi)$ (see Fig. 1). As the response tensors are symmetric in the first two indices, the independent tensor elements for the B-linear longitudinal (transverse) responses are $\chi_{xx;x}$ and $\chi_{xx;y}$ ($\chi_{yx;x}$ and $\chi_{yx;y}$). The fourth rank tensor $\chi_{ab;cd}$ is symmetric in the first two (a, b) and the last two (c, d) indices. Hence, for the quadratic-B longitudinal (transverse) response $\chi_{xx;xx}$, $\chi_{xx;yy}$ and $\chi_{xx;xy}$ ($\chi_{yx;xx}$, $\chi_{yx;yy}$ and $\chi_{yx;xy}$) are the only independent elements. We present crystalline symmetry restrictions on these tensor elements for nonmagnetic and magnetic systems in Table I and Table S1 of the Supplemental Material [47], respectively. An interesting conclusion from our symmetry analysis is that the presence of $\mathcal{C}_{3z}$ symmetry does not restrict any of the 2DPHE response tensors. This makes hexagonal systems such as multi-layered graphene, transition metal dichalcogenides, and their twisted moiré heterostructures good candidates to observe 2DPHE. We now focus on the angular variation of the 2DPHE current.

Angular variation of the 2DPHE currents—The variation of the 2DPHE currents with the planar angle between the $\boldsymbol{E}$ and $\boldsymbol{B}$ is important for exploring its origin and the relative contribution of different terms. We work with the field configuration described in Fig. 1 to obtain the longitudinal and transverse 2DPHE currents: $j^{\mathrm{2DPHE}}_{\parallel(\perp)} = \sigma_{\parallel(\perp)}E_{\parallel}$. We calculate the angular dependence of the 2DPHE conductivities to be

$$\sigma_{\parallel} = \tau B(\chi_{xx;x}\cos\phi + \chi_{xx;y}\sin\phi) + \tau B^2(\chi_{xx;xx}\cos^2\phi + \chi_{xx;yy}\sin^2\phi + \chi_{xx;xy}\sin\phi\cos\phi), \tag{9}$$

$$\sigma_{\perp} = \tau B(\chi_{yx;x}\cos\phi + \chi_{yx;y}\sin\phi) + \tau B^2(\chi_{yx;xx}\cos^2\phi + \chi_{yx;yy}\sin^2\phi + \chi_{yx;xy}\sin\phi\cos\phi). \tag{10}$$

These equations and the symmetry restrictions in Table I (and Table S1 in Supplemental Material [47]) provide a complete characterization of the 2DPHE responses. For nonmagnetic systems with an in-plane mirror ($\mathcal{M}_x$ or $\mathcal{M}_y$) or an in-plane twofold rotation ($\mathcal{C}_{2x}$ or $\mathcal{C}_{2y}$) symmetry, the longitudinal (transverse) response is entirely captured by $\chi_{xx;xx}$, and $\chi_{xx;yy}$ ($\chi_{yx;xy}$) with the conventional $\cos^2\phi$ ($\sin 2\phi$) angular dependence [55]. For more details, please refer to Sec. S8 of the Supplemental Material [47].

2DPHE in gated bilayer graphene—To demonstrate the 2DPHE in a realistic system, we consider the tight-binding model of Bernal stacked bilayer graphene (BLG). It offers the natural advantage of being readily available, and its doping and layer asymmetry can be tuned via the combination of top and bottom gate voltages. The Hamiltonian of pristine BLG with a vertical displacement field possesses $\mathcal{T}$ and $\mathcal{C}_{3z}$ symmetry, while it breaks $\mathcal{P}$ symmetry. Owing to the presence of $\mathcal{T}$ symmetry, only the B^2 contributions to the 2DPHE in BLG are allowed. The breakdown of $\mathcal{P}$ symmetry is crucial for inducing a planar BC and planar OMM in systems with $\mathcal{T}$ symmetry. BLG also has a mirror symmetry about its armchair direction along $\hat{\boldsymbol{y}}$, which is represented by $\mathcal{M}_x$ (see Fig. S4 of the Supplemental Material [47]). The $\mathcal{M}_x$ symmetry of BLG dictates that only the $\chi_{yx;xy}$ component can be finite with the $\sin 2\phi$ angular dependence in $\sigma_{\perp}$. To explore the role of other planar Hall contributions $\propto B^2$ ($\chi_{yx;xx}$ and $\chi_{yx;yy}$), we break the $\mathcal{M}_x$ symmetry of BLG by applying a uniaxial strain of 1% strength at an angle of 30° to the zigzag direction. The details of the strain implementation in the tight-binding model of BLG [6,57–62] are discussed in Sec. S6 of the Supplemental Material [47]. We present the band structure of strained BLG around one of the two valleys (K point) for interlayer potential $\Delta = 0.05$ eV in Fig. 2(a). In Fig. 2(b), we show the color plot of the density of states as a function of the chemical potential (μ) and Δ.

TABLE I. The symmetry restrictions of the longitudinal and planar Hall response tensors. The cross (✗) and the tick (✓) mark signify the corresponding response tensor is symmetry forbidden and allowed, respectively. The longitudinal and transverse PHE tensors in the same row have identical symmetry restrictions. Here, $\mathcal{M}_a$, $\mathcal{C}_{na}$, and $\mathcal{S}_{na}$ represent mirror, n-fold rotation, and n-fold roto-inversion symmetry operation along the a direction for $a = \{x, y, z\}$, respectively.

Longitudinal	Transverse	$\mathcal{P}$	$\mathcal{T}$	$\mathcal{PT}$	$\mathcal{M}_x$	$\mathcal{M}_y$	$\mathcal{M}_z$	$\mathcal{C}_{2x}$	$\mathcal{C}_{2y}$	$\mathcal{C}_{2z}$	$\mathcal{C}_{3z}$	$\mathcal{C}_{4z}$	$\mathcal{C}_{6z}$	$\mathcal{S}_{4z}$	$\mathcal{S}_{6z}$
$\chi_{xx;x}$	$\chi_{yx;y}$	✓	✗	✗	✓	✗	✗	✓	✗	✗	✓	✗	✗	✗	✓
$\chi_{xx;y}$	$\chi_{yx;x}$	✓	✗	✗	✗	✓	✗	✗	✓	✗	✓	✗	✗	✗	✓
$\chi_{xx;xx}$, $\chi_{xx;yy}$	$\chi_{yx;xy}$	✓	✓	✓	✓	✓	✓	✓	✓	✓	✓	✓	✓	✓	✓
$\chi_{xx;xy}$	$\chi_{yx;xx}$, $\chi_{yx;yy}$	✓	✓	✓	✗	✗	✓	✗	✗	✓	✓	✓	✓	✓	✓

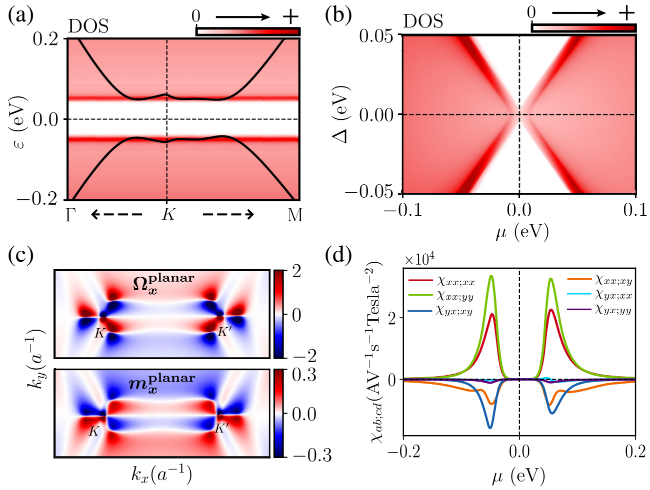

FIG. 2. (a) Electronic band structure of strained BLG around the K point, with the background color showing the density of states (DOS) in the unit of $a^{-2}\,\mathrm{eV}^{-1}$. (b) The variation of DOS with chemical potential μ and the interlayer potential Δ in (b). (c) The upper (lower) panel shows the k-space distribution of the x component of the planar BC (OMM) for the first conduction band in the unit of a^2 $[(e/\hbar)a^2 \cdot \mathrm{eV}]$, where a is the lattice constant. (d) Different components of 2DPHE response tensors $\chi_{ab;cd}$ as a function of μ evaluated at temperature $T = 50$ K. In (a), (c), and (d) we used the interlayer potential $\Delta = 0.05$ eV.

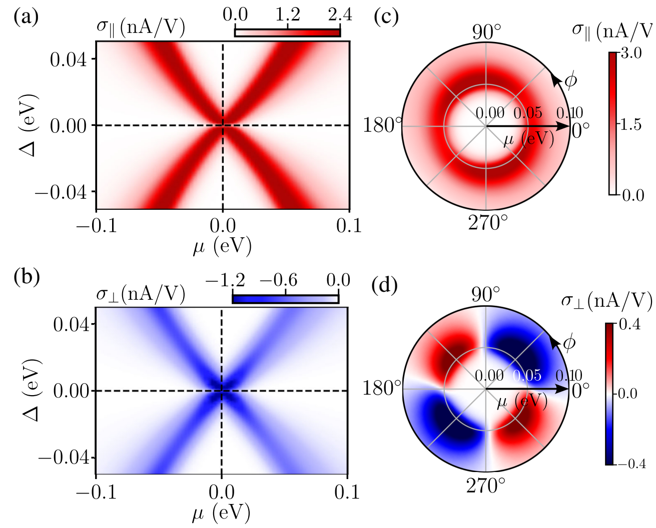

FIG. 3. The color plot of the (a) longitudinal and (c) transverse 2DPHE conductivities in $\mu - \Delta$ space for strained BLG. These parameters can be experimentally tuned via the top and back gates. We have chosen the $B = 1$ T, $\phi = 60°$, $\tau = 100$ fs [66] and temperature $T = 50$ K. The angular dependence of the (b) longitudinal and (d) transverse 2DPHE conductivities. The small deviation from $\sigma_\parallel \propto \cos^2\phi$ and $\sigma_\perp \propto \sin(2\phi)$ dependence is induced by the strain-induced mirror symmetry breaking. In the angular plots, we have $\Delta = 0.05$ eV.

For BLG, the out-of-plane position operator is given by the matrix $\hat{\mathcal{Z}} = (c/2)\tau_z \otimes \sigma_0$. σ_0 is the identity matrix for the sublattice space, and τ_z is the Pauli matrix in the layer space. Here, $c \approx 3.35$ Å is the interlayer distance. We use this in Eqs. (1) and (2) to calculate the planar BC and planar OMM. We present the x component of planar BC and planar OMM for the first conduction band in Fig. 2(c). The y components of these quantities are presented in Fig. S5 of Supplemental Material [47,63].

We numerically calculate the 2DPHE responses of BLG, illustrating their dependence on the chemical potential μ in Fig. 2(d). In contrast to $\chi_{xx;xx}$, $\chi_{xx;yy}$, and $\chi_{yx;xy}$, which remain finite even in the presence of $\mathcal{M}_x$ symmetry, the contributions $\chi_{xx;xy}$, $\chi_{yx;xx}$, and $\chi_{yx;yy}$ require $\mathcal{M}_x$ symmetry breaking to be finite. As a consequence, these contributions are relatively smaller in magnitude. We highlight that all the 2DPHE response tensors are pronounced in the vicinity of the band edges, where the planar band geometric quantities have a hot spot [see Fig. 2(c)]. Interestingly, the peak in the responses near the band edge arises from the Van Hove singularity in the density of states, which is a marker of the Lifshitz transitions in BLG (see Sec. S7 of the Supplemental Material [47] for more details).

We present color plots of the variation of $\sigma_\parallel$ and $\sigma_\perp$ with μ and Δ in Figs. 3(a) and 3(b). Both the conductivities have appreciable values only in the vicinity of the band edges, highlighting the band-geometric nature of 2DPHE. The peaks in both $\sigma_\perp$ and $\sigma_\parallel$ reflect the Van Hove singularity in the DOS, marked by the dark regions in Fig. 2(b). We present the angular variation of $\sigma_\parallel$ and $\sigma_\perp$, as μ is varied, in the polar color plots in Figs. 3(c) and 3(d). We highlight that the angular variation of the 2DPHE responses deviates from the conventional $\sigma_\parallel \propto \cos^2\phi$ and $\sigma_\perp \propto \sin 2\phi$ dependence due to the strain-induced mirror symmetry breaking [65].

Experimental implications—For estimating the feasibility of measuring 2DPHE responses in experiments, we consider an in-plane magnetic field of $B = 1$ T, $\phi = 60°$ and $\tau = 100$ fs [66]. With these parameters, $\sigma_\perp$ ($\sigma_\parallel$) becomes $\sim 2.3(8.0)$ $\mathrm{AV}^{-1}\,\mathrm{m}^{-1}$ in BLG. Here, we have converted conductivities to the conventional 3D unit using the layer thickness of BLG. Assuming a sample size of ~ 10 μm and a moderate electric field of $E \sim 1$ V/μm, we estimate the planar Hall voltage to be $V_\perp \sim 0.03$ V (see Sec. S8 of Supplemental Material [47]), which is well within experimental reach. In experiments, a much smaller magnitude of response (voltage ∼ nanovolt) can be measured. Additionally, we investigated the planar Hall response in bilayer WTe_2 [67–69], a system with naturally broken inversion symmetry. Our results show that the 2DPHE response in bilayer WTe_2 is larger than in bilayer graphene. However, it remains smaller than the experimentally measured PHE response in bulk WTe_2 [56] (see Sec. S9 of Supplemental Material [47] for details).

We now explore ways to distinguish the 2D planar Hall effect (2DPHE) from other in-plane magneto-Hall responses (see Sec. S10 of Supplemental Material [47] for details). Magnetic field-induced Berry curvature corrections to the anomalous Hall velocity can lead to in-plane magneto-Hall responses $\propto EB$ [25–29,31,70], while anisotropic spin scattering mechanisms also contribute to the planar Hall effect [32–39]. Both effects require strong spin-orbit coupling (SOC), with antisymmetric (or symmetric) response tensors for anomalous velocity (or spin scattering) contributions. In contrast, 2DPHE responses are symmetric and do not rely on SOC. Consequently, in layered 2D systems with SOC, such as transition metal dichalcogenides, the total symmetric planar response will have contributions from the 2DPHE and asymmetric spin scattering. However, the asymmetric spin scattering contribution is comparatively negligible in BLG due to its very small SOC strength. Hence, in multilayer graphene systems, 2DPHE dominates the planar magnetoresponse.

Conclusion—Our discovery of 2DPHE brings the vast class of layered 2D materials under the purview of planar Hall effect probes, which were limited to 3D materials. Additionally, 2DPHE offers a novel tool to probe the previously unexplored planar quantum-geometric properties of Bloch electrons in 2D materials. The existence of planar Berry curvature and orbital magnetic moment motivates the study of other novel phenomena [71,72], which were believed to be inaccessible in 2D materials. For instance, the planar Berry curvature can give rise to a vertical (perpendicular to the 2D plane) anomalous Hall effect in the linear and nonlinear response regimes. An interesting application of this is that vertical charge transport [73], with restricted out-of-plane carrier velocity, can induce a nonequilibrium interlayer electric polarization [74–76]. This may offer a novel way to control the switching of out-of-plane electric polarization in layered ferroelectric materials [77–80] via an in-plane electric field, with potential for new device applications.

Acknowledgments—We acknowledge many fruitful discussions with Adhip Agarwala (IIT Kanpur, India), Debottam Mandal (IIT Kanpur, India), and Atasi Chakraborty (Johannes Gutenberg University, Germany). K. G., S. D., and H. V. acknowledge the Ministry of Education, Government of India, for funding support through the Prime Minister's Research Fellowship.

[1] Le Khac Quynh, Nguyen The Hien, Nguyen Hai Binh, Tran Tien Dung, Bui Dinh Tu, Nguyen Huu Duc, and Do Thi Huong Giang, Simple planar Hall effect based sensors for low-magnetic field detection, Adv. Natl. Sci. **10**, 025002 (2019).

[2] K. L. Yau and J. T. H. Chang, The planar Hall effect in thin foils of Ni-Fe alloy, J. Phys. F **1**, 38 (1971).

[3] J. Li, S. L. Li, Z. W. Wu, S. Li, H. F. Chu, J. Wang, Y. Zhang, H. Y. Tian, and D. N. Zheng, A phenomenological approach to the anisotropic magnetoresistance and planar Hall effect in tetragonal $La_{2/3}Ca_{1/3}MnO_3$ thin films, J. Phys. Condens. Matter **22**, 146006 (2010).

[4] H. X. Tang, R. K. Kawakami, D. D. Awschalom, and M. L. Roukes, Giant planar Hall effect in epitaxial (Ga,Mn)As devices, Phys. Rev. Lett. **90**, 107201 (2003).

[5] M. Bowen, K.-J. Friedland, J. Herfort, H.-P. Schönherr, and K. H. Ploog, Order-driven contribution to the planar Hall effect in Fe_3Si thin films, Phys. Rev. B **71**, 172401 (2005).

[6] Brian T. Schaefer and Katja C. Nowack, Electrically tunable and reversible magnetoelectric coupling in strained bilayer graphene, Phys. Rev. B **103**, 224426 (2021).

[7] S. Nandy, Girish Sharma, A. Taraphder, and Sumanta Tewari, Chiral anomaly as the origin of the planar Hall effect in Weyl semimetals, Phys. Rev. Lett. **119**, 176804 (2017).

[8] Nitesh Kumar, Satya N. Guin, Claudia Felser, and Chandra Shekhar, Planar Hall effect in the Weyl semimetal GdPtBi, Phys. Rev. B **98**, 041103(R) (2018).

[9] Ming-Xun Deng, Hou-Jian Duan, Wei Luo, W. Y. Deng, Rui-Qiang Wang, and L. Sheng, Quantum oscillation modulated angular dependence of the positive longitudinal magnetoconductivity and planar Hall effect in Weyl semimetals, Phys. Rev. B **99**, 165146 (2019).

[10] Lei Li, Jin Cao, Chaoxi Cui, Zhi-Ming Yu, and Yugui Yao, Planar Hall effect in topological Weyl and nodal-line semimetals, Phys. Rev. B **108**, 085120 (2023).

[11] Da Ma, Hua Jiang, Haiwen Liu, and X. C. Xie, Planar Hall effect in tilted Weyl semimetals, Phys. Rev. B **99**, 115121 (2019).

[12] Kamal Das, Sahil Kumar Singh, and Amit Agarwal, Chiral anomalies induced transport in Weyl metals in quantizing magnetic field, Phys. Rev. Res. **2**, 033511 (2020).

[13] Yi-Wen Wei, Ji Feng, and Hongming Weng, Spatial symmetry modulation of planar Hall effect in Weyl semimetals, Phys. Rev. B **107**, 075131 (2023).

[14] Kamal Das and Amit Agarwal, Linear magnetochiral transport in tilted type-I and type-II Weyl semimetals, Phys. Rev. B **99**, 085405 (2019).

[15] Sunit Das, Kamal Das, and Amit Agarwal, Chiral anomalies in three-dimensional spin-orbit coupled metals: Electrical, thermal, and gravitational anomalies, Phys. Rev. B **108**, 045405 (2023).

[16] Shuo-Ying Yang, Jonathan Noky, Jacob Gayles, Fasil Kidane Dejene, Yan Sun, Mathias Dörr, Yurii Skourski, Claudia Felser, Mazhar Nawaz Ali, Enke Liu, and Stuart S. P. Parkin, Field-modulated anomalous Hall conductivity and planar Hall effect in $Co_3Sn_2S_2$ nanoflakes, Nano Lett. **20**, 7860 (2020).

[17] Rahul Ghosh and Ipsita Mandal, Direction-dependent conductivity in planar Hall set-ups with tilted Weyl/multi-Weyl semimetals, J. Phys. Condens. Matter **36**, 275501 (2024).

[18] Rahul Ghosh and Ipsita Mandal, Electric and thermoelectric response for Weyl and multi-Weyl semimetals in planar Hall configurations including the effects of strain, Physica (Amsterdam) **159E**, 115914 (2024).

[19] David Rakhmilevich, Fei Wang, Weiwei Zhao, Moses H. W. Chan, Jagadeesh S. Moodera, Chaoxing Liu, and Cui-Zu Chang, Unconventional planar Hall effect in exchange-coupled topological insulator–ferromagnetic insulator heterostructures, Phys. Rev. B **98**, 094404 (2018).

[20] S. Nandy, A. Taraphder, and Sumanta Tewari, Berry phase theory of planar Hall effect in topological insulators, Sci. Rep. **8**, 14983 (2018).

[21] Di Xiao, Ming-Che Chang, and Qian Niu, Berry phase effects on electronic properties, Rev. Mod. Phys. **82**, 1959 (2010).

[22] J. Cayssol and J. N. Fuchs, Topological and geometrical aspects of band theory, J. Phys. **4**, 034007 (2021).

[23] Kamal Das and Amit Agarwal, Intrinsic Hall conductivities induced by the orbital magnetic moment, Phys. Rev. B **103**, 125432 (2021).

[24] Rhonald Burgos Atencia, Amit Agarwal, and Dimitrie Culcer, Orbital angular momentum of Bloch electrons: Equilibrium formulation, magneto-electric phenomena, and the orbital Hall effect, Adv. Phys. **9**, 2371972 (2024).

[25] Vladimir A. Zyuzin, In-plane Hall effect in two-dimensional helical electron systems, Phys. Rev. B **102**, 241105(R) (2020).

[26] James H. Cullen, Pankaj Bhalla, E. Marcellina, A. R. Hamilton, and Dimitrie Culcer, Generating a topological anomalous Hall effect in a nonmagnetic conductor: An in-plane magnetic field as a direct probe of the Berry curvature, Phys. Rev. Lett. **126**, 256601 (2021).

[27] Raffaele Battilomo, Niccoló Scopigno, and Carmine Ortix, Anomalous planar Hall effect in two-dimensional trigonal crystals, Phys. Rev. Res. **3**, L012006 (2021).

[28] Tian Liang, Jingjing Lin, Quinn Gibson, Satya Kushwaha, Minhao Liu, Wudi Wang, Hongyu Xiong, Jonathan A. Sobota, Makoto Hashimoto, Patrick S. Kirchmann, Zhi-Xun Shen, R. J. Cava, and N. P. Ong, Anomalous Hall effect in $ZrTe_5$, Nat. Phys. **14**, 451 (2018).

[29] Jiadong Zhou *et al.*, Heterodimensional superlattice with in-plane anomalous Hall effect, Nature (London) **609**, 46 (2022).

[30] Song Sun, Hongming Weng, and Xi Dai, Possible quantization and half-quantization in the anomalous Hall effect caused by in-plane magnetic field, Phys. Rev. B **106**, L241105 (2022).

[31] Hui Wang, Yue-Xin Huang, Huiying Liu, Xiaolong Feng, Jiaojiao Zhu, Weikang Wu, Cong Xiao, and Shengyuan A. Yang, Orbital origin of the intrinsic planar Hall effect, Phys. Rev. Lett. **132**, 056301 (2024).

[32] A. A. Taskin, Henry F. Legg, Fan Yang, Satoshi Sasaki, Yasushi Kanai, Kazuhiko Matsumoto, Achim Rosch, and Yoichi Ando, Planar Hall effect from the surface of topological insulators, Nat. Commun. **8**, 1340 (2017).

[33] Oliver Breunig, Zhiwei Wang, A. A. Taskin, Jonathan Lux, Achim Rosch, and Yoichi Ando, Gigantic negative magnetoresistance in the bulk of a disordered topological insulator, Nat. Commun. **8**, 15545 (2017).

[34] Pan He, Steven S.-L. Zhang, Dapeng Zhu, Yang Liu, Yi Wang, Jiawei Yu, Giovanni Vignale, and Hyunsoo Yang, Bilinear magnetoelectric resistance as a probe of three-dimensional spin texture in topological surface states, Nat. Phys. **14**, 495 (2018).

[35] Bin Wu, Xing-Chen Pan, Wenkai Wu, Fucong Fei, Bo Chen, Qianqian Liu, Haijun Bu, Lu Cao, Fengqi Song, and Baigeng Wang, Oscillating planar Hall response in bulk crystal of topological insulator Sn doped $Bi_{1.1}Sb_{0.9}Te_2S$, Appl. Phys. Lett. **113**, 011902 (2018).

[36] Pan He, Steven S.-L. Zhang, Dapeng Zhu, Shuyuan Shi, Olle G. Heinonen, Giovanni Vignale, and Hyunsoo Yang, Nonlinear planar Hall effect, Phys. Rev. Lett. **123**, 016801 (2019).

[37] Shi-Han Zheng, Hou-Jian Duan, Jia-Kun Wang, Jia-Yu Li, Ming-Xun Deng, and Rui-Qiang Wang, Origin of planar Hall effect on the surface of topological insulators: Tilt of Dirac cone by an in-plane magnetic field, Phys. Rev. B **101**, 041408 (2020).

[38] Wen Rao, Yong-Long Zhou, Yong-jia Wu, Hou-Jian Duan, Ming-Xun Deng, and Rui-Qiang Wang, Theory for linear and nonlinear planar Hall effect in topological insulator thin films, Phys. Rev. B **103**, 155415 (2021).

[39] Wei Ai, Fuyang Chen, Zhaochao Liu, Xixi Yuan, Lei Zhang, Yuyu He, Xinyue Dong, Huixia Fu, Feng Luo, Mingxun Deng, Ruiqiang Wang, and Jinxiong Wu, Observation of giant room-temperature anisotropic magnetoresistance in the topological insulator β-Ag_2Te, Nat. Commun. **15**, 1259 (2024).

[40] Enrico Drigo and Raffaele Resta, Chern number and orbital magnetization in ribbons, polymers, and single-layer materials, Phys. Rev. B **101**, 165120 (2020).

[41] Daisuke Hara, M. S. Bahramy, and Shuichi Murakami, Current-induced orbital magnetization in systems without inversion symmetry, Phys. Rev. B **102**, 184404 (2020).

[42] Kyoung-Whan Kim, Hogyun Jeong, Jeongwoo Kim, and Hosub Jin, Vertical transverse transport induced by hidden in-plane Berry curvature in two dimensions, Phys. Rev. B **104**, L081114 (2021).

[43] Dinh Loc Duong, Seok Joon Yun, and Young Hee Lee, van der Waals layered materials: Opportunities and challenges, ACS Nano **11**, 11803 (2017).

[44] Pratap Chandra Adak, Subhajit Sinha, Amit Agarwal, and Mandar M. Deshmukh, Tunable moiré materials for probing Berry physics and topology, Nat. Rev. Mater. **9**, 481 (2024).

[45] Raffaello Bianco and Raffaele Resta, Orbital magnetization as a local property, Phys. Rev. Lett. **110**, 087202 (2013).

[46] Si-Si Wang, Yi-Ming Dai, Hui-Hui Wang, Hao-Can Chen, Biao Zhang, and Yan-Yang Zhang, Orbital magnetization under electric field and orbital magnetoelectric polarizability for a bilayer chern system, Phys. Rev. B **107**, 125135 (2023).

[47] See Supplemental Material at http://link.aps.org/supplemental/10.1103/PhysRevLett.134.026301, which includes Refs. [12,14,21,48–50], for detailed discussion on (S1) the derivation of planar BC and planar OMM expressions, (S2) the out-of-plane position operator, (S3) general expression for planar BC and planar OMM and analytical calculation of them for 2×2 low-energy bilayer graphene model, (S4) the detailed derivation of longitudinal and planar Hall response tensors, (S5) the details of symmetry analysis, (S6) the strain implementation in the tight-binding model for bilayer graphene and y components of planar Berry curvature and OMM, (S7) the Van Hove singularity and Lifshitz transition of Fermi surface, (S8) experimental implications and estimation of planar Hall voltage, (S9) planar Hall response in bilayer WTe_2, and (S10) other in-plane magneto-Hall responses in two-dimensional systems.

[48] Ganesh Sundaram and Qian Niu, Wave-packet dynamics in slowly perturbed crystals: Gradient corrections and Berry-phase effects, Phys. Rev. B **59**, 14915 (1999).

[49] Naoto Nagaosa, Jairo Sinova, Shigeki Onoda, A. H. MacDonald, and N. P. Ong, Anomalous Hall effect, Rev. Mod. Phys. **82**, 1539 (2010).

[50] D. T. Son and B. Z. Spivak, Chiral anomaly and classical negative magnetoresistance of Weyl metals, Phys. Rev. B **88**, 104412 (2013).

[51] Sheng-Chin Ho, Ching-Hao Chang, Yu-Chiang Hsieh, Shun-Tsung Lo, Botsz Huang, Thi-Hai-Yen Vu, Carmine Ortix, and Tse-Ming Chen, Hall effects in artificially corrugated bilayer graphene without breaking time-reversal symmetry, National electronics review **4**, 116 (2021).

[52] Kamal Das and Amit Agarwal, Thermal and gravitational chiral anomaly induced magneto-transport in Weyl semimetals, Phys. Rev. Res. **2**, 013088 (2020).

[53] Robert E. Newnham, *Properties of Materials: Anisotropy, Symmetry, Structure* (Oxford University Press, New York, 2005).

[54] Samuel V. Gallego, Jesus Etxebarria, Luis Elcoro, Emre S. Tasci, and J. Manuel Perez-Mato, Automatic calculation of symmetry-adapted tensors in magnetic and non-magnetic materials: A new tool of the Bilbao Crystallographic Server, Acta Crystallogr. Sect. A **75**, 438 (2019).

[55] In some papers, the planar Hall effect refers to the odd in ϕ contribution to the transverse current-voltage, which is proportional to $\sin\phi\cos\phi$. However, some other works such as Refs. [10,11,13,37,56], use the term planar Hall response to include the $\sin^2\phi$ or $\cos^2\phi$ contributions as well which are even in ϕ, as long as the applied electric field, magnetic field, and the voltage-current generated are in the same plane. In this Letter, we follow this terminology to refer to the Hall components proportional to $\cos^2\phi$ and $\sin^2\phi$, along with the $\sin\phi\cos\phi$ responses to be the planar Hall response.

[56] Peng Li, Chenhui Zhang, Yan Wen, Long Cheng, George Nichols, David G. Cory, Guo-Xing Miao, and Xi-Xiang Zhang, Anisotropic planar Hall effect in the type-II topological Weyl semimetal WTe_2, Phys. Rev. B **100**, 205128 (2019).

[57] Edward McCann and Mikito Koshino, The electronic properties of bilayer graphene, Rep. Prog. Phys. **76**, 056503 (2013).

[58] Vitor M. Pereira, A. H. Castro Neto, and N. M. R. Peres, Tight-binding approach to uniaxial strain in graphene, Phys. Rev. B **80**, 045401 (2009).

[59] Seon-Myeong Choi, Seung-Hoon Jhi, and Young-Woo Son, Controlling energy gap of bilayer graphene by strain, Nano Lett. **10**, 3486 (2010).

[60] Jen-Hsien Wong, Bi-Ru Wu, and Ming-Fa Lin, Strain effect on the electronic properties of single layer and bilayer graphene, J. Phys. Chem. C **116**, 8271 (2012).

[61] A. B. Kuzmenko, I. Crassee, D. van der Marel, P. Blake, and K. S. Novoselov, Determination of the gate-tunable band gap and tight-binding parameters in bilayer graphene using infrared spectroscopy, Phys. Rev. B **80**, 165406 (2009).

[62] Gerardo G Naumis, Salvador Barraza-Lopez, Maurice Oliva-Leyva, and Humberto Terrones, Electronic and optical properties of strained graphene and other strained 2d materials: A review, Rep. Prog. Phys. **80**, 096501 (2017).

[63] We emphasize that these quantities are not $\mathcal{C}_{3z}$ symmetric even without any in-plane strain [42,64]. However, they are valley contrasting due to the global $\mathcal{T}$-symmetry of BLG.

[64] Rui-Chun Xiao, Ding-Fu Shao, Wenjuan Huang, and Hua Jiang, Electrical detection of ferroelectriclike metals through the nonlinear Hall effect, Phys. Rev. B **102**, 024109 (2020).

[65] This is a consequence of the strain-induced $\mathcal{M}_x$ symmetry breaking, which makes $\chi_{xx;xy}, \chi_{yx;xx}$, and $\chi_{yx;yy}$ components finite, modifying the angular dependence following Eqs. (9) and (10).

[66] M. Monteverde, C. Ojeda-Aristizabal, R. Weil, K. Bennaceur, M. Ferrier, S. Guéron, C. Glattli, H. Bouchiat, J. N. Fuchs, and D. L. Maslov, Transport and elastic scattering times as probes of the nature of impurity scattering in single-layer and bilayer graphene, Phys. Rev. Lett. **104**, 126801 (2010).

[67] Z. Z. Du, C. M. Wang, Hai-Zhou Lu, and X. C. Xie, Band signatures for strong nonlinear Hall effect in bilayer WTe_2, Phys. Rev. Lett. **121**, 266601 (2018).

[68] Chuanchang Zeng, Snehasish Nandy, A. Taraphder, and Sumanta Tewari, Nonlinear nernst effect in bilayer WTe_2, Phys. Rev. B **100**, 245102 (2019).

[69] Qiong Ma, Su-Yang Xu, Huitao Shen, David MacNeill, Valla Fatemi, Tay-Rong Chang, Andrés M Mier Valdivia, Sanfeng Wu, Zongzheng Du, Chuang-Han Hsu *et al.*, Observation of the nonlinear Hall effect under time-reversal-symmetric conditions, Nature (London) **565**, 337 (2019).

[70] Huiyuan Zheng, Dawei Zhai, Cong Xiao, and Wang Yao, Layer coherence origin of intrinsic planar Hall effect in 2d limit, arXiv:2402.17166.

[71] Juncheng Li, Dawei Zhai, Cong Xiao, and Wang Yao, Dynamical chiral Nernst effect in twisted van der Waals few layers, Quantum Front. **3**, 11 (2024).

[72] Dawei Zhai, Cong Chen, Cong Xiao, and Wang Yao, Time-reversal even charge Hall effect from twisted interface coupling, Nat. Commun. **14**, 1961 (2023).

[73] Archana Tiwari, Fangchu Chen, Shazhou Zhong, Elizabeth Drueke, Jahyun Koo, Austin Kaczmarek, Cong Xiao, Jingjing Gao, Xuan Luo, Qian Niu, Yuping Sun, Binghai Yan, Liuyan Zhao, and Adam W. Tsen, Giant c-axis nonlinear anomalous Hall effect in Td-$MoTe_2$ and WTe_2, Nat. Commun. **12** (2021).

[74] Ying Xiong, Mark S. Rudner, and Justin C. W. Song, Anti-screening and nonequilibrium layer electric phases in graphene multilayers, Phys. Rev. Lett. **133**, 136901 (2024).

[75] Yang Gao, Yinhan Zhang, and Di Xiao, Tunable layer circular photogalvanic effect in twisted bilayers, Phys. Rev. Lett. **124**, 077401 (2020).

[76] Oles Matsyshyn, Ying Xiong, Arpit Arora, and Justin C. W. Song, Layer photovoltaic effect in van der Waals heterostructures, Phys. Rev. B **107**, 205306 (2023).

[77] Zhiren Zheng, Qiong Ma, Zhen Bi, Sergio de la Barrera, Ming-Hao Liu, Nannan Mao, Yang Zhang, Natasha Kiper, Kenji Watanabe, Takashi Taniguchi, Jing Kong, William A. Tisdale, Ray Ashoori, Nuh Gedik, Liang Fu, Su-Yang Xu, and Pablo Jarillo-Herrero, Unconventional ferroelectricity in moiré heterostructures, Nature (London) **588**, 71 (2020).

[78] Xirui Wang, Kenji Yasuda, Yang Zhang, Song Liu, Kenji Watanabe, Takashi Taniguchi, James Hone, Liang Fu, and Pablo Jarillo-Herrero, Interfacial ferroelectricity in rhombohedral-stacked bilayer transition metal dichalcogenides, Nat. Nanotechnol. **17**, 367 (2022).

[79] Kenji Yasuda, Xirui Wang, Kenji Watanabe, Takashi Taniguchi, and Pablo Jarillo-Herrero, Stacking-engineered ferroelectricity in bilayer boron nitride, Science **372**, 1458 (2021).

[80] Zaiyao Fei, Wenjin Zhao, Tauno A. Palomaki, Bosong Sun, Moira K. Miller, Zhiying Zhao, Jiaqiang Yan, Xiaodong Xu, and David H. Cobden, Ferroelectric switching of a two-dimensional metal, Nature (London) **560**, 336 (2018).